SLOVAK UNIVERSITY OF TECHNOLOGY IN BRATISLAVA
Faculty of Civil Engineering

Ing. Peter Špánik

Dissertation thesis abstract

Carrier phase multipath modelling in short-term positioning

to acquire the academic title *philosophiae doctor (PhD.)*
in the doctoral study programme
3636 Geodesy and Cartography, full-time study

Bratislava 2021

Dissertation thesis has been prepared in full-time study at Department of Global Geodesy and Geoinformatics, Faculty of Civil Engineering, Slovak University of Technology in Bratislava.

PhD. student: Ing. Peter Špánik
Department of Theoretical Geodesy and Geoinformatics
Faculty of Civil Engineering, SUT in Bratislava
Radlinského 11, 810 05 Bratislava (Slovakia)

Supervisor: doc. Ing. Renata Ďuračiová, PhD.
Department of Theoretical Geodesy and Geoinformatics
Faculty of Civil Engineering, SUT in Bratislava
Radlinského 11, 810 05 Bratislava (Slovakia)

Consultant: assoc. prof. Ing. Luis García-Asenjo, PhD.
Department of Cartographic Engineering, Geodesy and Photogrammetry
Universitat Politècnica de València
Camino de Vera s/n, 46022 Valencia (Spain)

Opponents: prof. Ing. Jan Kostelecký, DrSc.[1,2]
[1] Department of Geomatics
Czech Technical University in Prague, Faculty of Civil Engineering
Thákurova 7, 166 29 Prague 6 (Czech Republic)
[2] Research Institute of Geodesy, Topography and Cartography, v.v.i
Ústecká 98, 250 66 Zdiby (Czech Republic)

doc. Ing. Michal Kačmařík, Ph.D.
Department of Geoinformatics
Faculty of Mining and Geology, Technical University of Ostrava
17. listopadu 2172/15, 708 00 Ostrava-Poruba (Czech Republic)

Ing. Branislav Droščák, PhD.
Department of Geodetic control
Geodetic and Cartographic Institute in Bratislava
Chlumeckého 4, 827 45 Bratislava (Slovakia)

The executive summary was sent on: ....

The dissertation defence takes place on: ....
at the Department of Theoretical Geodesy and Geoinformatics, Faculty of Civil Engineering, Slovak University of Technology in Bratislava, Radlinského 11, 810 05 Bratislava.

....
prof. Ing. Stanislav Unčík, PhD.
The dean of the Faculty of Civil Engineering
Slovak University of Technology in Bratislava
Radlinského 11, 810 05 Bratislava

Abstrakt

Predkladaná dizertačná práca sa zaoberá efektom viaccestného šírenia sa signálu v meraniach pomocou globálnych navigačných družicových systémov (angl. GNSS). Tento efekt stále ostáva najväčším nemodelovaným rušivým efektom pôsobiacim na stanovisku. Efekt viaccestného šírenia sa signálu sa prejavuje v kódových aj fázových meraniach GNSS. V kódových meraniach je efekt v ráde niekoľkých metrov a je závislý najmä od kvality prijímača. V prípade fázových meraní je efekt v ráde centimetrov, ale môže byť značne zosilnený pri použití kombinácie meraní. Podstatou problému viaccestného šírenia sa signálu je, že ho nie je možné znížiť postupom diferencovania, ktorý je využívaný pri relatívnom určovaní polohy. V teoretickej časti práce sme sa zamerali na opis odrazu elektromagnetického signálu z fyzikálneho hľadiska, ktorý je podkladom pre jednotlivé metódy detekcie odrazených signálov, pričom v práci sú bližšie popísané dve metódy detekcie: pomocou výpočtu rezíduí dvojnásobných diferencií a detekcia s využitím kombinácie hodnôt pomeru signálu a šumu (SNR). V praktickej časti sme sa venovali spracovaniu meraní z permanentnej stanice pre ktorú bola vypočítaná a aplikovaná korekčná mapa fázového multipathu. Aplikáciou takejto korekcie sme dosiahli zvýšenie presnosti a úspešnosti riešenia ambiguít. Druhou praktickou časťou je odhad a aplikácia kalibrácie hodnôt SNR ktorá slúžila na detekciu efektu multipath v mestskom prostredí. Naše výsledky ukazujú, že po odstránení identifikovaných meraní je možné zvýšiť polohovú presnosť určenia bodu pri kinematickom móde zhruba o 20%. Jedným z výsledkov práce je aj voľne dostupný GNSS-toolbox v programovacom jazyku MATLAB. Toolbox bol využitý na všetky výpočty v rámci práce a môže nájsť svoje uplatnenie ako v praktickej tak i akademickej oblasti.

Abstract

Proposed dissertation thesis deals with multipath effect in measurements of Global Navigation Satellite System (GNSS). Even today multipath effect represents the biggest non-modelled station dependent error source. Multipath affects both, the code and phase measurements. In case of code measurement, impact is in order of meters and strongly depends on the receiver quality. For the phase measurements it is in order of centimeters, but can be highly amplified when using signal combinations. The nature of the multipath problem for phase measurements is that it can not be simply reduced by differentiation approach widely used in precise relative positioning. In the theoretical part of thesis we have focused on physical description of signal reflection process, what serve as solid basic for practical part where we exploit two multipath detection methods: first one uses uses double-difference residuals, second uses connection between phase multipath and combination of Signal to Noise Ratio values (SNR) for various carrier waves. We performed experimental measurements to test both methods. For double-difference residuals method we made measurement close to permanent station to derive multipath correction map. After applying such estimated correction map we were able to improve position estimates as well as increase successful ambiguity fixing ratio. For the second method we performed SNR calibration in open field and subsequently we use such calibration for multipath detection in urban environment. We were able to remove majority of reflected signals what leads to improved positioning results in kinematic mode by about 20%. One of the thesis outcomes is also freely available MATLAB programming package GNSS-toolbox. Package was used for all numerical computations mentioned in the thesis and can be be further used in practical or academic sector.

Contents

Preface

Position determination using space geodesy techniques, especially GNSS, is well established method for precise positioning of points on the Earth's surface. Different techniques involving utility of continuously operating reference station networks at regional, local or national level or satellite based augmentation systems (abbreviated as SBAS) are used to increase accuracy and reliability of obtained results. Nowadays there is nothing extraordinary for professional surveyors to perform Real time kinematic surveys (abbreviated as RTK) with centimeter level accuracy as often declared by correction providers. Unfortunately with this increased usage popularity of GNSS receivers in surveying practice we can even often see that surveyors use GNSS equipment like so called „black boxes“. When we work with GNSS receiver we have to bear in mind all the weaknesses of this positioning method. We have to realize that GNSS signals processed by receiver are extremely weak and vulnerable to interference. We have to be careful especially when we are working in harsh environment like e.g. urban areas or forests. In such environments GNSS signals can reflect from surrounding objects and then are tracked by GNSS receiver in the same manner like the direct one. GNSS receiver can only partially distinguish between direct and reflected signal. In fact receiver process all signals from one satellite together as one composed signal, what leads to incorrect measurement. English term for this reflected signal effect is *multipath*. It refers to fact that the signal can find multiple ways or paths how to get into GNSS antenna.

This thesis is divided into four major parts. The aim of the first part is to understand and describe the process of electromagnetic signal reflection from the theoretical point of view. We described how the signal interacts with material, how the material properties influence reflection and how signal properties are changed after reflection. Second part of thesis deals with topics of how reflected signal affects GNSS code, phase and SNR measurements. The effect of GNSS equipment parameters is commented here. The core of the thesis is the third part focused on description of two methods which are able to detect multipath effect in GNSS measurements. First method is based on double-difference residuals applicable in post-processing mode, second one, based on anomalous behaviour in SNR measurements is ready for real-time use. Both methods have been tested during experimental measurements and obtained results are presented. The last two parts are dedicated to dissertation thesis outcomes.

1 Prior research in field of phase multipath effect

Research in the field of multipath effect can be tracked back to the mid 90s when research institutions across the world starts to discover potential benefits of precise GPS. One of the first papers dealing with multipath topic is (Bishop et al., 1985) where authors identified multipath contamination in determination of absolute ionospheric time delays.

Authors also performed tests with artificial vertical plane reflector and suggest low-pass and sidereal filtering to reduce its effect. In (Evans et al., 1986) and (Georgiadou and Kleusberg, 1988) authors shows strong correlation between ionospheric residuals obtained from consecutive days in different observation environments. Repetitive residual pattern was attributed to the reflection from surrounding of the antenna due to repeating satellite-receiver geometry.

Further advances in receiver technology in early 2000s have resulted in improved mitigation of code multipath (e.g. using Multipath Estimation Delay Lock Loop technique in Novatel receivers (Fenton and Townsend, 1994), (Townsend et al., 1995) or Everest Multipath rejection technology in Trimble receivers), however no such general improvement, was achieved for carrier-phase multipath. Addressing of the carrier-phase multipath issues seems to be extremely challenging from the signal processing point of view, for that reasons majority of the research papers which deal with carrier-phase multipath is focused on in-situ multipath reduction (tailored for specific site) and are mostly done in post-processing mode.

In (Wanninger and May, 2001) authors propose extraction of carrier-phase multipath correction from network of base GPS stations in Germany. Network data in time span of one year were used to compute carrier-phase residuals on each GPS carrier as well as for widelane and ionosphere-free combination which after averaging served as correction values. Improvement in order of 10% for short baselines (∼1km) was achieved for ionosphere-free linear combination. For other scenarios non-modelled differential ionospheric errors seems to be prevalent source of errors. In (Dilssner et al., 2008) and (Wübbena et al., 2011) authors were focused on estimation of near-field multipath component which is strongly influenced by antenna mount and material of the top pillar plate under the antenna. Authors uses Automated Absolute Antenna Field Calibration Technique (developed by Geo++ company) with combination of additional antenna installed closely to investigated antenna. Additional antenna was put on high pole in distance ∼10 m from tested antenna and serve as a reference for forming double-differenced carrier phases. Near-field multipath corrections were estimated along with antenna phase center variation values. Several scenarios and most common antenna setups were tested and authors shown that even for geodetic-grade surveying antennas near-field effect can introduce carrier-phase errors between 1-2 cm for mid-latitude locations and biases up to 4-5 cm in polar regions.

Different approach to model carrier-phase correction on the site is to simulate signal reflection using 3D model of antenna surroundings. In paper (Lau and Cross, 2007) authors suggest to use ray-tracing method and accounts for effects like antenna gain pattern, wave polarization change and surface attenuation. Such complex model shows good agreement to the double-differenced residuals obtained in various test environments, mostly using only planar reflectors. Similarly in (Nicolas et al., 2011) authors uses ray-tracing technique to simulate satellite signal. In this case the model of the environment comes from terrestrial laser scanner, so it has significantly better quality than in previously mentioned paper. However only SNR values comparison was made, not the actual measurement residuals. Results shows fairly good agreement of general trend in SNR values, however well-known periodic pattern in SNR values was not simulated properly. It could suggest that the wave polarization change in reflection process was not properly handled in simulation (no detailed information were provided in that paper). Different multipath simulation technique was used in (Fan and Ding, 2006). Authors used as basis Geometrical Theory of Diffraction method. Testing in real urban environment was performed and test results shown that up to 34% errors in the carrier phase observation were reduced.

Major drawback of the 3D model simulation methods is that it require the multipath environment to be known apriori the measurement. First linkage between SNR values and carrier-phase multipath can be found in paper (Comp and Axelrad, 1998). In-depth details about the dependency between SNR and carrier-phase multipath values will be revealed in section 3.3. Authors utilize SNR values to adaptively estimate the spectral parameters (frequency, amplitude, phase offset) of multipath and then constructs a profile of the multipath error in the carrier phase. A multipath correction is subsequently made by subtracting the profile from the actual phase measurement data. The technique is demonstrated on several test cases while special receiver setup with four antennas attached was used. Averaging performance of reducing the carrier-phase multipath error by 47% was achieved. In the further works of (Bilich et al., 2008) and (Bilich and Larson, 2008) the same team used wavelet analysis to initialize an adaptive least squares process to solve for time-varying multipath parameters. As test environment perfectly flat, salt plane was used. With ordinary setup where one antenna was placed on tripod and the other one was laid on the ground authors achieved ∼20% reduction in post-fit residuals RMS for low elevation angles (data below 20° elevation). Simplified version of SNR multipath correction was used in (Rost and Wanninger, 2009) when only constant value of attenuation factor $\alpha = 0.3$ was used. As test environment the urban parkplace was selected while park surface should serve as major reflector. RMS values across all double-differenced residuals experienced a reduction of approximately 25% when multipath corrections were applied. In (Strode and Groves, 2016) novel technique was used to detect multipath using combination of SNR values on all three available GPS carrier frequencies. Method is in more details presented in section 4.2 also with its potential extensions and drawbacks.

For real-time application, the signal path calculation within the 3D model can be slow. For such uses cases more simple detection method for reflected or non-line of sight (NLOS) signals should be used. Typical use case is kinematic positioning of the car in urban environment where buildings obscure significant portion of the sky. The aim of the method in such cases is to label the satellite and exclude it from further positioning solution. In paper (Suzuki and Kubo, 2015) authors uses publicly available Google Earth API and well known image classification algorithms to create satellite visibility mask which serve for detection if signal comes directly from the satellite or it is NLOS signal. In (Tongleamnak and Nagai, 2017) authors uses single zenith pointing fish-eye camera and image classification to create such satellite visibility mask. Additionally in (Moreau et al., 2017) authors uses two fish-eye zenith pointing cameras to create using simple 3D model of antenna surroundings to be to detect NLOS as well as reflected signals.

Another way how to suppress multipath at the GNSS site is to use an absorption foam material placed underneath the antenna. In (Elósegui et al., 1995) authors revealed systematic influence in double-difference carrier phase residuals which was dependent on satellite elevation angle. Approach to reduced this systematic multipath effect using ray optics finds authors as insufficient and propose to embed microwave absorbing material Eccosorb HR-2 with a thickness of 5 cm to the top steel plane of the antenna pillar. Several configurations were tested: two layers of absorber instead of one; absorber extended bellow the diameter of the pillar instead of tailored to it; absorber covering only the steel plate embedded in the pillar and not the concrete pillar itself. All proved to be comparably effective at reducing long frequency scattering of residuals. Additional effort by (Kerkhoff et al., 2010) used arrangement of radio frequency absorbing foam blocks placed under antenna in reverse pyramidal shape as a matter to reduce multipath from elevation near the horizon and below. Absorbing material Cuming Microwave C-RAM AR of 10 cm thickness rated for outdoor use was used reducing the RMS error of post-fit residuals by 24% for code and almost 17% for carrier phase observations. In (Yang et al., 2016) authors shows different arrangement of antenna wave-absorbing shield in form of concave disc covered by layer of pyramidal microwave absorber. Authors performed comparison of code-ranging precision on two permanent sites for GPS, GLONASS and Beidou. Result show improvement between 17% to 36% on code pseudorange RMS post-fit error, which suggest that this design of multipath shield can be the best option, however effect of wave-absorbing shield on carrier-phase measurements was not evaluated in the paper.

2 Thesis objectives

The main objective of the thesis is to test methods for multipath detection and subsequent mitigation of multipath contamined observations in GNSS positioning with emphasis in short-term observation sessions. According this goal several specific partial objectives were identified, to accomplish the main objective. These specific objectives are following:

- Make summary of the prior research in the field of GNSS multipath detection and mitigation with emphasis on the methods which can be used in short-term positioning.
- Perform mapping of phase multipath environment at selected GNSS permanent station using the method of double-differenced phase residuals. Measurement session has to be made with GNSS equipment similar to the equipment at selected permanent station.
- Test antenna environment modification using shield of radio-frequency absorbing foam to reduce multipath effect. To evaluate the impact of such site modification experimental measurements with and without absorbing foam needs to be made.
- Enhance the phase multipath detection method based on SNR combination first described by Strode and Groves (2016), identify multipath events in measurements and exclude them from processing.

3 Signal reflection impact on GNSS measurements

In concept, the satellite navigation observables are ranges which are deduced from measured time or phase difference based on a comparison between received signals and receiver-generated signals. Unlike the terrestrial electronic distance measurements, GNSS uses the „one-way concept“ where two clocks are involved, namely one in the satellite and the other in the receiver. Thus, the ranges are biased by satellite and reciver clock errors and, consequently, they are denoted as pseudoranges (Hofmann-Wellenhof et al., 2008). According to method, how we determine the pseudorange, we recognize code pseudoranges and phase pseudoranges. Both of these pseudoranges are somehow affected by reflected signals. The induced effect of reflected signals in pseudorange's value is called multipath effect.

3.1 Signal reflection impact on code pseudoranges

To acquire a signal, the receiver generates a replica of known pseudorange code and attempts to align it with the incoming code by sliding the replica in time and computing the correlation. Structure of pseudo-random code sequences (PRN) for each satellite is given in interface control document, e.g. for GPS it is IS-GPS-200H (US Department of Defence, 2013). Auto-correlation of PRN code is very high and exhibits a sharp peak when the replica is aligned with the code received from the satellite. Once the satellite signal is acquired, time alignment offset τ is determined and receiver start to track the signal. Code tracking is implemented as a feedback control loop called a *delay lock loop*, which continuously adjusts the replica code to keep it aligned with the code in incoming signal. During code tracking, receiver can not distinguish direct and reflected signal. Effect of reflected signal will produce new correlation maximum moved by offset $\Delta\tau = \tau_M - \tau$, where τ_M is instant of reflected signal reception. Magnitude of new correlation maximum is always lower than correlation maximum of direct signal, because of reflection losses. Example reflected signal correlation is shown on Fig. 1.

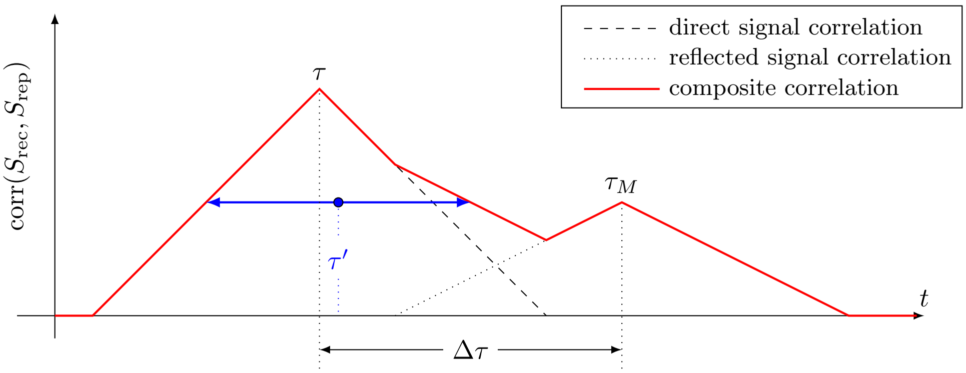

FIGURE 1: Correlation of received signal S_{rec} and receiver generated replica S_{rep}. Time alignment offset τ is influenced by reflected signal given by time offset $\Delta\tau$. Interference can be constructive ($\tau' > \tau$) or destructive ($\tau' < \tau$).

Multipath effect on code pseudoranges is affected by receiver parameters (correlator width) and parameters of signal itself (mainly chip length T_c – time duration of 1 bit in receiving code). Manufacturers usually does not make their correlator's setting available to public, however we can summarize that narrower correlator is more robust to multipath effect. Correlator width varies from 1 chip length in cheap navigational boards to 0.05 chip in geodetic quality receivers. Many of geodetic receivers apply also multicorrelator principle with early, prompt, and late replica correlation to get more reliable results (Misra and Enge, 2011). From signal side, it is convenient to have shorter chip length and there exist inverse relation between signal bandwidth B and code chip length as $B = 2/T_c$. This means that wide bandwidth codes (e.g. GPS P or L5 code, Galileo E5) are more robust to multipath effect than signals with narrower bandwidth (Hofmann-Wellenhof et al., 2008). Evaluation of multipath effect in code pseudoranges is usually done by so called *multipath observable* abbreviated as *MP*. This variable is simple combination of code and phase measurements on two or alternatively even three carrier frequencies in the following form:

$$MP^i_{jk} = R_i - \Phi_j + \frac{\lambda_i^2 + \lambda_j^2}{\lambda_j^2 - \lambda_k^2}(\Phi_j - \Phi_k) - B \tag{1}$$

where R is code measurement, Φ is phase measurement, B is bias due to unknown ambiguities and i, j, k denotes frequencies. Computation with (1) is possible, but cycle-slips have to be detected previously. For ambiguous character of MP values, we more often use its time variability expressed as RMS to detect code multipath. Formula for computation is implemented in applications like teqc (Estey and Meertens, 1999), G-Nut/Anubis (Vaclavovic and Douša, 2013) or MultipathAnalysis (Špánik, 2015).
Because of not significant use of code pseudoranges in precise static and kinematic geodetic positioning, code multipath study plays only marginal role in this thesis. However, code measurements are extensively used in Precise Point Positioning method (PPP), thus even code multipath is interesting from this point of view. Also some techniques for ambiguity resolution rely on code and phase combination, e.g. Melbourne-Wübbena widelane combination which is used in Bernese software for long baselines (Dach et al., 2015). During studies I have investigated impact of reflection material properties in station environment using MP combination, for more details see (Špánik and Gerhátová, 2016).

3.2 Signal reflection impact on phase pseudoranges

Phase pseudorange, or phase measurement, denoted as Φ is difference between the phases of the receiver-generated carrier signal and the carrier received from a satellite at the instant of the measurement. This measurement is acquired in receiver processor after PRN code sequence is removed from received signal by delay lock loop. Removal leaves the carrier modulated only by the navigation message. Signal is then tracked with another feedback control loop called *phase lock loop*. Essentially, the receiver generates a sinusoidal signal to match the frequency and phase of the incoming signal, and simultaneously extract the navigation message bits (Misra and Enge, 2011). Incoming composite signal s_c is formed as composition of one strong direct signal s_d and one or n weaker reflected signals s_r (in case of more reflected signals, i-th signal is denoted as $s_r^{(i)}$). More intensive reflected signal s_r, bigger the influence on composite phase determination it has. In phase measurements the path delay Δd of reflected signal is transformed into the phase shift $\Delta\Phi_{d,r}$ between direct and reflected signal (also denoted as relative phase). This shift corresponds to remainder after subtraction of integer number of carrier wavelengths from path delay according to (without denoting i-th signal index):

$$\Delta\Phi_{d,r} = \frac{(\Delta d - n\lambda)\, 2\pi}{\lambda} \tag{2}$$

This phase shift is in radians and its value vary $\Delta\Phi_{d,r} \in \langle 0,\, 2\pi \rangle$ as path delay Δd change with satellite movement in the sky. For direct, reflected and composite signal we can write down equations according to (Rost and Wanninger, 2009):

$$s_d = A_d \cos \Phi_d \tag{3}$$

$$s_r^{(i)} = \alpha_i \, A_d \cos\left(\Phi_d + \Delta\Phi_{d,r}^{(i)}\right) \tag{4}$$

$$s_c = s_d + s_r \tag{5}$$

$$s_c = A_d \cos \Phi_d + \sum_{i=1}^{n} \alpha_i \, A_d \cos\left(\Phi_d + \Delta\Phi_{d,r}^{(i)}\right)$$

where A_d represents amplitude of direct signal. Reflected signal is attenuated by α, where $0 \leq \alpha \leq 1$. This attenuation coefficient includes absolute reflection coefficients of surface's material, wave-to-antenna coupling factor F and also antenna gain. For each of reflected signals it may has different value, thus it is denoted as α_i. Carrier-phase multipath $\Delta\Phi_m$ in GNSS measurements is defined by simple equation:

$$\Delta\Phi_m = \Phi_c - \Phi_d \tag{6}$$

where Φ_c is composite phase (what is measured) and Φ_d is the direct phase (what we want to measure). According to attenuation coefficient α, the phase multipath $\Delta\Phi_m$ may acquires various values. In the worst case theoretical scenario where amplitude of direct and reflected signal are equal and thus $\alpha = A_r/A_d = 1$, values of phase multipath are $\Delta\Phi_m \in \langle -\lambda/4, +\lambda/4 \rangle$. In case of GPS L1 carrier it represents $\Delta\Phi_m \in \langle -47.6, +47.6 \rangle$ mm, for GPS L2 carrier it is $\Delta\Phi_m \in \langle -61.1, +61.1 \rangle$ mm, which are not negligible values in precise relative positioning. For derivation of phase multipath equation, phasor

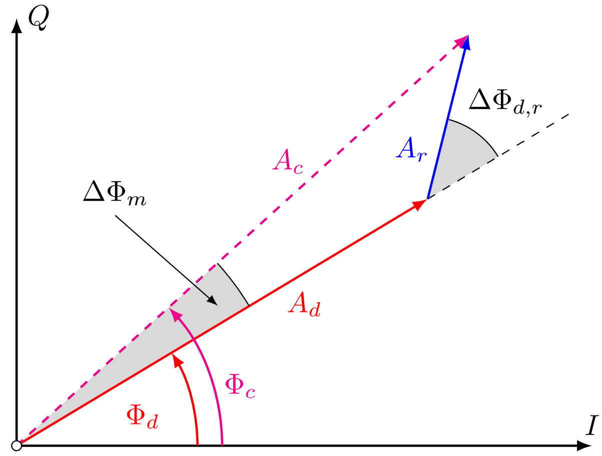

FIGURE 2: Phasor diagram of carrier phase determination: in-phase I and quadrature phase Q components of direct signal (A_d, Φ_d), reflected signal ($A_r = \alpha A_d$, $\Delta\Phi_{d,r}$ and the resulting composite signal (A_c, Φ_c). The carrier-phase error due to multipath is labelled $\Delta\Phi_m$.

representation on Fig. 2 is convenient. In phase lock loop, resulting carrier phase is gained from in-phase I and quadrature phase Q components as $\Phi_c = \tan^{-1}(Q_c/I_c)$. Equation for phase multipath $\Delta\Phi_m$ (7) is gathered from geometrical relations as following:

$$\Delta\Phi_m = \tan^{-1}\left(\frac{\alpha \cdot \sin\Delta\Phi_{d,r}}{1 + \alpha \cdot \cos\Delta\Phi_{d,r}}\right) \tag{7}$$

In precise positioning methods we rarely use only single frequency measurements. Different frequency combinations are used to remove disturbing effects of atmosphere or for purposes of ambiguity resolution. Linear combination can be defined as: $\Phi^x = a_x\Phi_1 + b_x\Phi_2$, where a_x, b_x are coefficients that define the relation between the observables and Φ_1, Φ_2 are the observables (Teunissen and Montenbruck, 2017). For phase multipath error in certain combination $\Delta\Phi^x_m$ we can write (8), a_x, b_x can be found in (Leick, 2004).

$$\Delta\Phi^x_m = a_x\Delta\Phi_{m,1} + b_x\Delta\Phi_{m,2} \tag{8}$$

3.3 Signal reflection impact on SNR quality measurements

The notation SNR represents a generic term for signal quality and is defined as the ratio of signal power S to noise power N (both in watts), measured at the same time and place in a circuit. The signal and noise power can be estimated during the correlation between the received and replicated signal. The main part of noise originates from the receiver electronics and the electromagnetic radiation from the sky, ground and objects in the close antenna's vicinity. Thermal noise is assumed to be white noise (Langley, 1997). Intuitively, the larger the SNR, the better the signal quality is. SNR is usually obtained using signal power S_{corr} and noise power N_{corr} of the modulated signal at the correlator output. However to assess the quality of a received GPS signal, the so-called carrier-to-noise ratio ($\text{CNR} = C/N$) is preferred, which makes use of the signal power C_{ant} and noise power N_{ant} of the unmodulated carrier at the receiving antenna (Kaplan and Hegarty, 2006). From the receiver antenna to correlator output, GNSS signals may be amplified by a factor of about 10^{10}, so that S_{corr} is significantly larger than C_{ant}. Nevertheless, according to the fact that the signal and noise powers are amplified by approximately the same factor, $S_{\text{corr}}/N_{\text{corr}}$ and $C_{\text{ant}}/N_{\text{ant}}$ are almost identical:

$$\text{CNR} = \frac{C}{N} = \frac{C_{\text{ant}}}{N_{\text{ant}}} \approx \frac{S_{\text{corr}}}{N_{\text{corr}}} = \frac{S}{N} = \text{SNR} \tag{9}$$

For GNSS signals, S is several magnitudes lager than N. Therefore, SNR values are usually expressed in terms of the logarithmic decibel (dB) scale as:

$$\text{SNR}\,[\text{dB}] = 10 \cdot \log_{10}(\text{SNR}) \tag{10}$$

In addition, noise power N can be written as the product of noise power density N_0 and loop bandwidth B_L – phase lock loop receiver parameter (Misra and Enge, 2011):

$$N\,[\text{W}] = N_0\,[\text{W/Hz}] \cdot B_L\,[\text{Hz}] \tag{11}$$

When substituting equation (11) to (9), we get SNR normalized to a specific bandwidth of 1 Hz and (10) becomes:

$$\begin{aligned} \text{SNR}\,[\text{dB}] &= 10 \cdot \log_{10} \frac{S}{N_0 \cdot B_L} = 10 \cdot \log_{10} \frac{S}{N_0} - 10 \cdot \log_{10}(B_L) \\ &= \text{SNR}_0\,[\text{dBHz}] - B_L\,[\text{dBHz}] \end{aligned} \tag{12}$$

where SNR_0 is called signal-to-noise power density ratio. It plays a key role in analysing GNSS receiver performance and is directly related to the precision of pseudo-range and carrier-phase observations (Langley, 1997). For moderate to strong signals, the corresponding SNR_0 should be larger than 35 dBHz (Hofmann-Wellenhof et al., 2008). Most high-end GNSS receivers deliver SNR_0 of up to 50 dBHz. Using the minimum received signal strength of $S = -158.5$ dBW (US Department of Defence, 2013) and a typical value for noise power density of $N_0 = -204$ dBW/Hz (US Department of Defence, 2013), a nominal SNR_0 of 45.5 dBHz is obtained. In geodetic community, SNR_0 measurements are often abbreviated as SNR, but as seen from previous relation, its meaning is different. However, to be concise with other research publications I will further use term

SNR, or general signal-to-noise ratio for SNR_0 values with units of dBHz. In fact, SNR measurements are affected by various factors (Misra and Enge, 2011):

1. shape of receiver's antenna gain pattern ,
2. the satellite antenna transmission gain,
3. changes in path loss due to the varying satellite-receiver distance (spreading),
4. variations in atmospheric attenuation,
5. signal power losses in preamplifier, antenna cable and receiver subsystems.

3.4 Link between signal quality and carrier phase multipath

Close connection between signal quality and carrier-phase multipath can be shown on phasor diagram on Fig. 2. The phase lock loop attempts to track a composite signal which is the vector sum of all phasors (direct plus multipath signal(s)). According to this, the SNR then becomes a measurement of composite signal amplitude, $\mathrm{SNR} \approx A_c$ (Bilich and Larson, 2008). Using the law of cosines and geometric relationships, composite SNR due to the direct signal plus single multipath reflection can be expressed as:

$$\mathrm{SNR}^2 \approx A_c^2 = A_d^2 + A_r^2 + 2A_dA_r \cos \Delta\Phi_{d,r} \tag{13}$$

Note that A_c is maximized when $\Delta\Phi_{d,r} = 0°$, A_c is minimal when $\Delta\Phi_{d,r} = 180°$ and A_c is close to the amplitude of direct signal when $\Delta\Phi_{d,r} = 90°$ or $270°$. This orthogonality of SNR values and carrier phase multipath error can be reviewed in four cases as shown on the Fig. 3 (Lau and Cross, 2006).

Case a) when the reflected signal is in-phase with the direct signal (Fig. 3a), the amplitude of reflected signal is added to the amplitude of direct signal and therefore the signal strength of the composite signal is maximized, which leads to the measured SNR greater than the nominal SNR. However it has zero phase shift ($\Delta\Phi_{d,r} = 0°$) and thus zero carrier phase error due to multipath ($\Delta\Phi_m = 0°$).

Case b) maximal carrier-phase error occurs (when assumed that α is up to 0.5) when the direct signal phasor and reflected signal phasor are orthogonal (Fig. 3b). This maximize phase of the composite signal relative to the direct signal and thus maximizes the carrier-phase error. Orthogonal phase shift ($\Delta\Phi_{d,r} = 90°$ or $270°$) leads to the maximum carrier phase error ($\Delta\Phi_m = \max$) due to multipath (value depends on α coefficient). In this case, the measured SNR is close to the nominal SNR because the amplitudes of direct and composite signals are similar.

Case c) when the reflected signal is out-of-phase with the direct signal (Fig. 3c), the amplitude of the multipath signal is subtracted from the amplitude of the direct signal, and therefore the signal strength of the composite signal is minimal which lead to lower SNR value when compared with nominal. It has the maximum phase shift ($\Delta\Phi_{d,r} = 180°$) but zero carrier-phase error ($\Delta\Phi_m = 0°$) due to multipath.

Case d) is the absolute worst case (Fig. 3d) when theoretical maximum carrier phase error $\Delta\Phi_m \to 90°$ can be achieved. It occurs when the amplitude of the multipath signal is equal to the amplitude of direct signal, and the phase shift $\Delta\Phi_{d,r} \to 180°$.

However, this almost never occurs in reality as the receiver normally simply loses lock when the direct signal strength is equal to or not much greater than reflected signal strength.

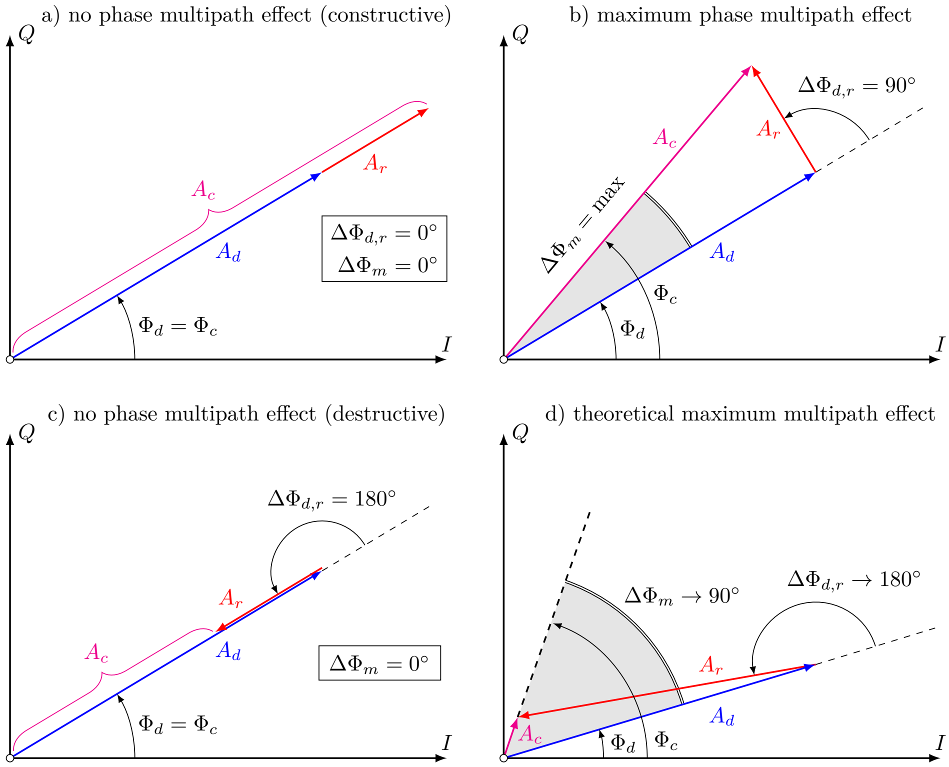

FIGURE 3: Phasor diagrams of phase multipath effect on amplitude of composite signal A_c. As seen on figures carrier phase multipath error $\Delta\Phi_m$ has orthogonal relation to anomalous SNR values (when SNR is close to its nominal values, corresponding to direct signal, $\Delta\Phi_m$ is maximal and otherwise).

4 Measurement's based GNSS multipath detection

This chapter form the main part of thesis. In the following subchapters two methods of phase multipath detection and mitigation based on GNSS measurements will be described. First method is build on interpretation of double-differenced residuals. For this method we have to know coordinates of analyzed station precisely, thus it is usable only for post-processing applications and possible multipath calibration of site. The second method is based on combination SNR quality measurements and is suitable for usage also in real-time. Methods were tested in various setups and results will be presented here.

4.1 Multipath detection via double differenced phase residuals

In Lau and Cross (2007), the method to extract the values of phase multipath for each satellite in each measurement's epoch is proposed. This method is based on computation of double differenced phase residuals $\Delta\Phi^{j,k}_{res}$ between two satellites j, k and for two nearby sites A, B. Maximal length of baseline should be up to 500 meters, due to cancellation of majority of disruptive effects by double-differencing (ionosphere and troposphere delays, satellite and receiver clock biases will be cancelled). Only small variations, in range of few tens of millimeters, are expected in double-differenced phase residuals. This variation is mainly caused by combination of phase multipath on sites A and B. The computation itself is based on subtraction of theoretical double-differenced geometrical distance $\Delta\rho^{j,k}_{A,B}$ from double-differenced carrier phases $\Delta\Phi^{j,k}_{A,B}$ acquired from measurements as (14).

$$\Delta\Phi^{j,k}_{A,B} - \Delta\rho^{j,k}_{A,B} = \Delta\Phi^{j,k}_{res} + N^{j,k}_{A,B} \tag{14}$$

Unfortunately the unknown double differenced ambiguity $N^{j,k}_{A,B}$ is unknown. If we assume no cycle slip during observation session we can expect integer values of individual ambiguity terms N^j_A, N^k_A, N^j_B, N^k_B and thus also integer value of $N^{j,k}_{A,B}$. Since we expect integer value of $N^{j,k}_{A,B}$ there should be constant shift between theoretical $\Delta\rho^{j,k}_{A,B}$ and measured double-differenced phase $\Delta\Phi^{j,k}_{A,B}$ with the size of several wavelengths, which can be estimated like mean shift value. Correctness of this estimation method can be verified by approximately zero mean value of residuals $\Delta\Phi^{j,k}_{res}$. Alternatively residuals would be out of expected maximal range $\langle -\lambda/4, +\lambda/4\rangle$ or measurements would contain cycle slip. For GLONASS system this approach can't be used because of different wavelengths for satellite j and k. In this case combined ambiguity term $N^{j,k}_{A,B}$ is not estimated, just mean value of $\Delta\Phi^{j,k}_{res} + N^{j,k}_{A,B}$ is subtracted to get double-differenced phase residuals.

4.1.1 Computation of double-differenced phase residuals

If we want to detect phase multipath variation in size of few tens of millimeters, precise information about used antennas, their position and orientation have to be apriori known to obtain reliable results. Relative position between sites A, B is more important than their absolute position in geocentric system. In the following, points A, B will be represented by mean antenna's phase centers (APC) belonging to used wavelength, not by any physical mark on the ground.
We will compare double-differenced geometric distance $\Delta\rho^{j,k}_{A,B}$ (obtained from precise ephemeris) with real measured values. If we compare non-differenced measurements it would cause an error, because measured phases are defined between receiver and satellites antenna's phase centers while IGS precise ephemeris are defined for satellite's center of mass (Kouba, 2009). In our case, this error will be fully cancelled by double differencing approach. On the receiver antenna side we have to take into account also phase center variation (PCV). This information can be found in ANTEX file and each geometric distance ρ^j_A, ρ^k_A, ρ^j_B, ρ^k_B have to be repaired by appropriate value before differencing. Only if two identic antennas without individual calibration are used, we can neglect this correction. For long baselines also satellite's phase center variation should be taken into account, but this is not our case since we assume short baseline here.

4.1.2 Relation between double-differenced residuals and phase multipath

Value of $\Delta\Phi^{j,k}_{res}$ consist of four individual phase multipath components in overall. This is due to double-differencing procedure when each one of four input phase measurements contains its own multipath component. We can put it together to write equation (15). Visualization of individual multipath components is shown on Fig. 4.

$$\Delta\Phi^{j,k}_{res} = \Delta\Phi^{j}_{m,A} - \Delta\Phi^{k}_{m,A} - \Delta\Phi^{j}_{m,B} + \Delta\Phi^{k}_{m,B} \tag{15}$$

Term $\Delta\Phi_{m,A}^{j}$ for example represents phase multipath for satellite j at site A. If we assume simplification that station A is situated in „low multipath environment“ ($\Delta\Phi_{m,A}^{j} \approx \Delta\Phi_{m,A}^{k} \approx 0$) and satellite j is close to zenith ($\Delta\Phi_{m,B}^{j} \approx 0$) then in equation (15) will remain only one non-zero multipath component at station B and for satellite k, thus $\Delta\Phi_{m,B}^{k} = \Delta\Phi_{res}^{j,k}$, thus phase multipath for single satellite at single station.

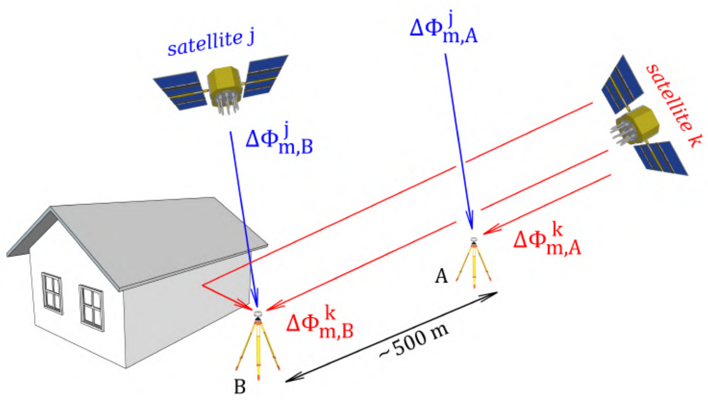

FIGURE 4: Individual phase multipath components of double-differenced phase measurement between two sites A, B and two satellites j, k.

4.1.3 Ground reflection mitigation with RF absorption foam

Reduction of ground reflections can be achieved using radio-frequency absorbing material placed beneath the antenna at reference site A. Several experiments shows utility of such approach as previously described in Chapter 1. In our tests we used sheets of radio-frequency absorption foam MAST MF22-0009-00 (see datasheet) with dimensions of 60 $\times$ 60 $\times$ 2.5 cm (Fig. 5). The foam is made of lightweight reticulated polyether and is suitable for our purpose since it absorbs electromagnetic signals in frequency range from 1 to 18 GHz. Foam can be used for internal as well as external installations, since in case of rain it can effectively transfer the water out of material due to its porous structure. Attenuation according the datasheet is on the level of -45 dB for whole frequency range including signals at high incident angles (it means that signals should be about 200-times weaker after passing or reflecting from the foam).

Sheets of absorption foam were placed on top of support structure as shown on Fig. 5. Absorption foam was touching bottom of the antenna mount on the level of the antenna reference point. Such placement should lead to attenuation of all signals coming from elevations below the horizon. Support structure is in close vicinity of the antenna, so to avoid signal interactions with the structure, it was made of wood. Central circular piece is placed on top of Zeiss tribrach and fixed in certain position to prevent rotation. Structure can be disassembled and re-used easily. Such design was chosen to allow utility of this structure during measurement campaigns, but can be used at permanent station as well. To keep foam sheets in place we used elastic rope and duct tape, which was enough to avoid misalignments due to weather conditions (e.g. wind).

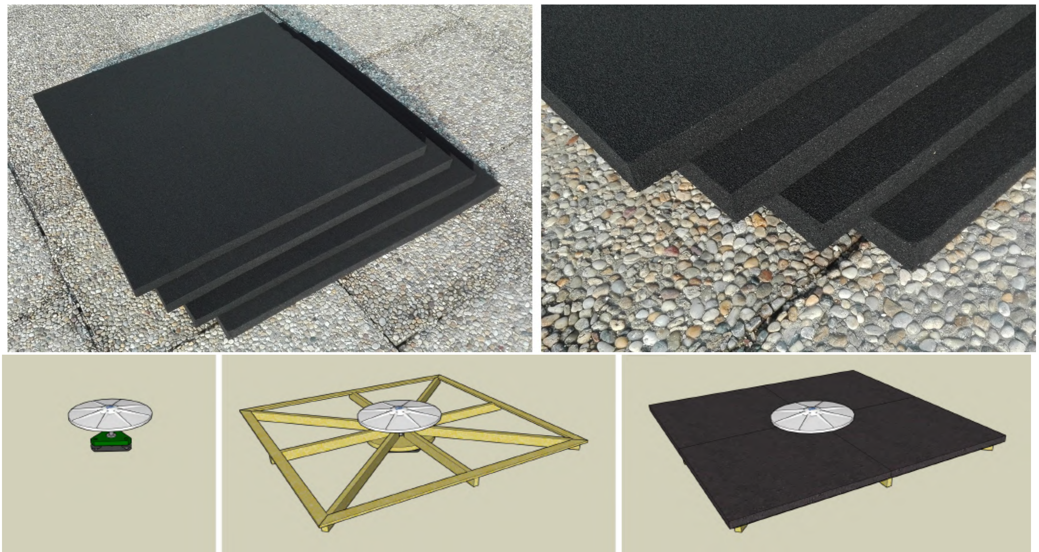

FIGURE 5: Sheets of used radio-frequency absorption foam (top) and design of portable wooden support structure (bottom)

4.1.4 Preliminary permanent site selection

To identify permanent stations with possible strong multipath influence we made analysis of MP quantity (described in 3.1) for all stations in SKPOS network. One day of observations in August 22, 2018 was used, since we want to get general overview about the code multipath environment at SKPOS stations and detailed station inspection was not our goal at this stage. For analysis we use the G-Nut/Anubis (Vaclavovic and Douša, 2013). Details about computation configuration can be found in conference paper (Špánik, 2018). Output XTR files were further processed and visualized with GNSS-toolbox. On the Fig. **??** we can see mean MP values from all SKPOS permanent stations sorted by its magnitude. For completeness also average values per antenna are plotted. From the overall multipath performance we can conclude that JABO (Jaslovské Bohunice) and GKU4 station require more attention and should be further studied. Since JABO station shows also significantly high number of cycle-slips it was selected as best candidate for computation of multipath correction using double-difference residuals approach.

4.1.5 Double differenced phase residuals computation at JABO site

For estimation of multipath correction map at permanent station JABO (Jaslovské Bohunice), setup with auxiliary GNSS site was used. Reference site A, where we do not expect any multipath influence, was realized by temporal tripod setup with attached radio-frequency absorbing foam structure. Temporal site A, for this experiment named as JAB1, was placed in open field with flat terrain in distance about 100 meters from JABO station. Simultaneous observations took place from 21. 9. 2019, 12:00 UT to 23. 9. 2019, 9:00 UT. Further information about sites are summarized in Table 1.

On the last day of the measurement we removed absorption foam structure at 7:25 UT to gather data for evaluation of the foam attenuation effect. Comparison of SNR values from two consecutive days was made for satellite GPS PRN 9. This satellite was chosen since it just start rising when absorption foam was removed from tripod setup. Comparison of SNR values on L1 carrier is plotted on Fig. 6. We can conclude that the amplitude of interferometric pattern on the SNR values increased about 30% when absorption foam was removed. For higher elevations (above 25 degrees) the effect of absorption foam seems to be negligible. This observation confirms that absorption foam can be used to reduce contamination of double-difference residuals by ground reflections, however we has to admit that the periodic pattern is still quite strong.

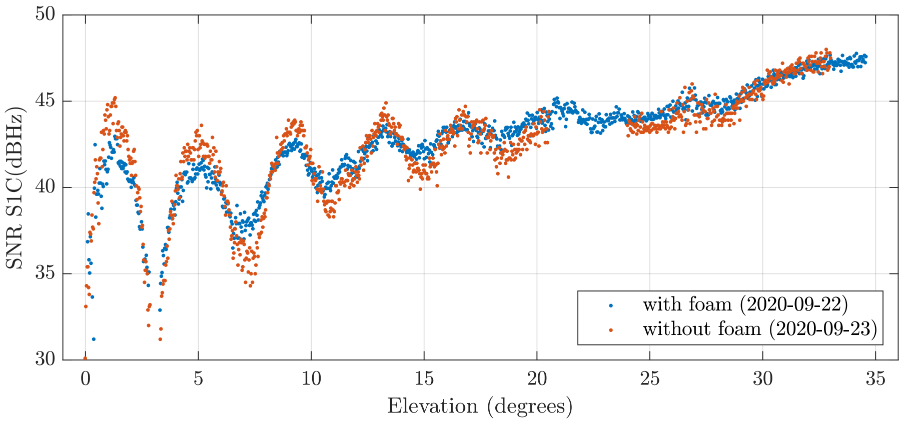

FIGURE 6: Effect of the absorption foam on the SNR for GPS PRN09.

Reference position of JABO station in ETRF2000 reference frame was used in experiment, similarly as it is used in SKPOS network solution. Height of JABO reference points was increased by 0.283 m to get coordinates of the JABO antenna reference point. Position of JAB1 ARP was computed from JABO ARP coordinates using static positioning mode with Trimble Business Centre software v5.21.

TABLE 1: Description of equipment used at JABO and JAB1 stations

Site	JABO	JAB1
Environment overview		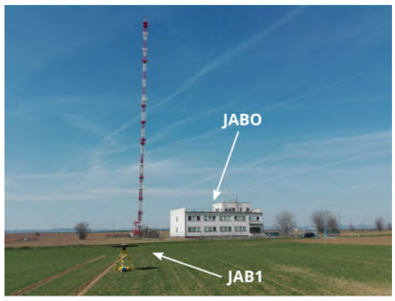
Calibration	individual (GPS+GLO, 15.2.2010)	NGS absolute (GPS+GLO)
Multipath reduction	none	absorption foam
Receiver	Trimble NetR9 (SN 5207K82278, v5.37)	Trimble NetR9 (SN 5448R50048, v5.37)
Antenna	TRM55971.00 NONE (SN 40932194)	TRM57971.00 NONE (SN 12118048)
Monumentation	steel mast on bearing wall	temporary on tripod
ARP position (ETRF2000)	X = 4035866.2000 m Y = 1285295.1408 m Z = 4753013.6119 m (used in SKPOS)	X = 4035921.4204 m Y = 1285355.7843 m Z = 4752936.8469 m (computed with TBC, v5.21)

4.1.6 Estimation of multipath correction map at JABO site

Correction map is represented by rectangular grid with equal step in azimuth and elevation. Angular resolution of 0.5° was selected. Each cell in the grid was computed from all double difference residuals found within the cell. If there are available residuals from more satellites, all of them are taken into account. Empty areas in the sky were interpolated via bilinear interpolation from closest cells to fill whole hemisphere. Multiple multipath correction maps were created, for each satellite system and frequency there is a separate map, there were totally 14 correction maps created (numbers in parenthesis represent number of available satellites with given signal):

- GPS observations: L1C (31), L2W (31), L2X (19) and L5X (12)
- Galileo observations: L1X (23), L5X (23), L7X (23) and L8X (23)
- GLONASS observations: L1C (20), L1P (20), L2C (20) and L2P (20)
- Beidou observations: L2I (11) and L7I (11)

Not whole observation period was taken into account when creating the correction maps. Only first 24 hours of continuous observation were taken and processed. The rest of the data was used for validation purpose. Quality of the correction map is related to the number of available satellites and their spatial distribution on the sky during measurement. Best quality correction maps were obtained for GPS L1C and L2W signals (Fig. 7) and for Galileo signals. Some grids, especially for Beidou system have low quality, since only small number of satellites was observed (there were only 9 healthy Beidou satellites available at the time of measurement). For these correction maps there are clear interpolation artifacts of the empty areas between individual satellite paths.

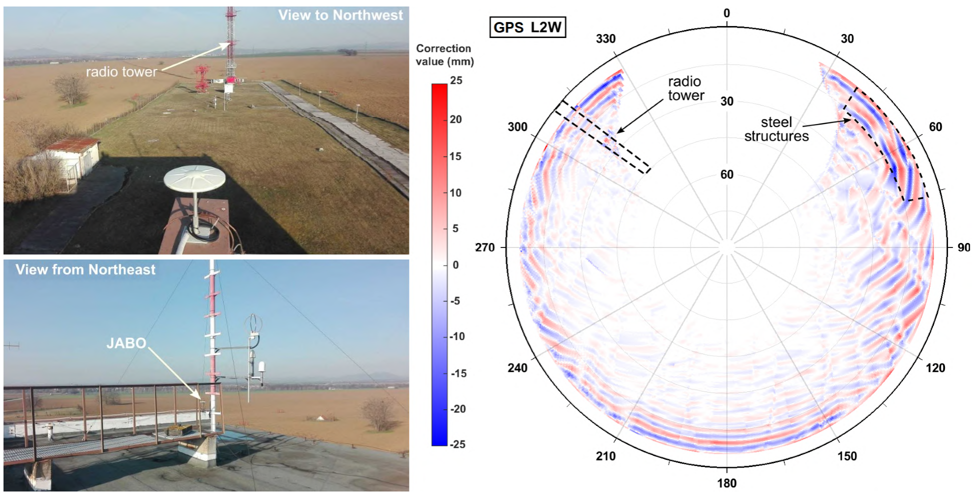

FIGURE 7: Photos of multipath sources at JABO site (left) and estimated multipath correction map for GPS L2W.

Identified regions with higher variability of residuals can be explained by reflection and refraction of the satellite signals from objects shown on Fig. 7. Variability of the residuals in the north-east region of the horizon can be explained by presence of the access bridge with steel railings which causes complex reflected and diffracted signal paths. Zone with higher variability of residuals in north-west region can be explained by signals diffraction from radio tower structure.

4.1.7 Evaluation of correction map effect at JABO site

Evaluation of the multipath correction maps was done on the same dataset as was used for correction map estimation, except that whole observation period was used and not only first 24 hours. Position of JABO station in ETRF2000 reference frame was estimated from JAB1 position using RTKLIB software (v2.4.3) in kinematic positioning mode and compared to JABO reference position from Table 1. RTKLIB employs extended Kalman filter in order to obtain the solution, further description of used procedure can be found in (Takasu, 2013). All available frequencies were used in processing together with precise ephemeris from GFZ. Also ionospheric and tropospheric delays were estimated together with station coordinates. Horizontal position scatter plots for all analyzed scenarions are shown on Fig. 8. Resulting ambiguity fixing success rate and achieved positioning precision is summarized in following table.

TABLE 2: Comparison of successful ambiguity fixes and solution precision for observation with and without applied multipath correction for different GNSS used (G=GPS, GR=GPS+GLONASS, GRE=GPS+GLONASS+Galileo).

GNSS used	Mask angle	Ambiguity fixed percentage		Solution standard deviations	
		No correction	Corrected	No correction	Corrected
GRE	5°	67.75%	71.05% (+3.30%)	$\sigma_n = 2.2$mm $\sigma_e = 1.7$mm $\sigma_u = 7.6$mm	$\sigma_n = 2.1$mm $\sigma_e = 1.6$mm $\sigma_u = 7.2$mm
	10°	99.27%	99.53% (+0.26%)	$\sigma_n = 2.0$mm $\sigma_e = 1.7$mm $\sigma_u = 6.5$mm	$\sigma_n = 1.8$mm $\sigma_e = 1.5$mm $\sigma_u = 6.0$mm
GR	5°	87.25%	88.27% (+1.03%)	$\sigma_n = 2.7$mm $\sigma_e = 2.1$mm $\sigma_u = 8.9$mm	$\sigma_n = 2.6$mm $\sigma_e = 1.9$mm $\sigma_u = 8.7$mm
	10°	99.81%	99.85% (+0.04%)	$\sigma_n = 2.6$mm $\sigma_e = 2.0$mm $\sigma_u = 7.6$mm	$\sigma_n = 2.4$mm $\sigma_e = 1.8$mm $\sigma_u = 7.1$mm
G	5°	96.92%	96.92% (+0.00%)	$\sigma_n = 3.4$mm $\sigma_e = 2.6$mm $\sigma_u = 9.8$mm	$\sigma_n = 3.2$mm $\sigma_e = 2.5$mm $\sigma_u = 10.5$mm
	10°	100.00%	100.00% (+0.00%)	$\sigma_n = 3.4$mm $\sigma_e = 2.4$mm $\sigma_u = 9.7$mm	$\sigma_n = 3.1$mm $\sigma_e = 2.3$mm $\sigma_u = 9.1$mm

From the Table 2 we can conclude that application of the multipath correction maps reduce position standard deviation in all tested scenarios up to 0.3 mm for horizontal and up to 0.6 mm for vertical component. Correction application seems to help most in the cases when the ambiguity success rate is not very successful, when GPS, GLONASS and Galileo systems are used together. Benefits of the correction application on ambiguity resolution are more noticeable in scenarios with lower elevation mask angle, which is according our expectations since most of multipath induced effects are caused by low elevation satellites.

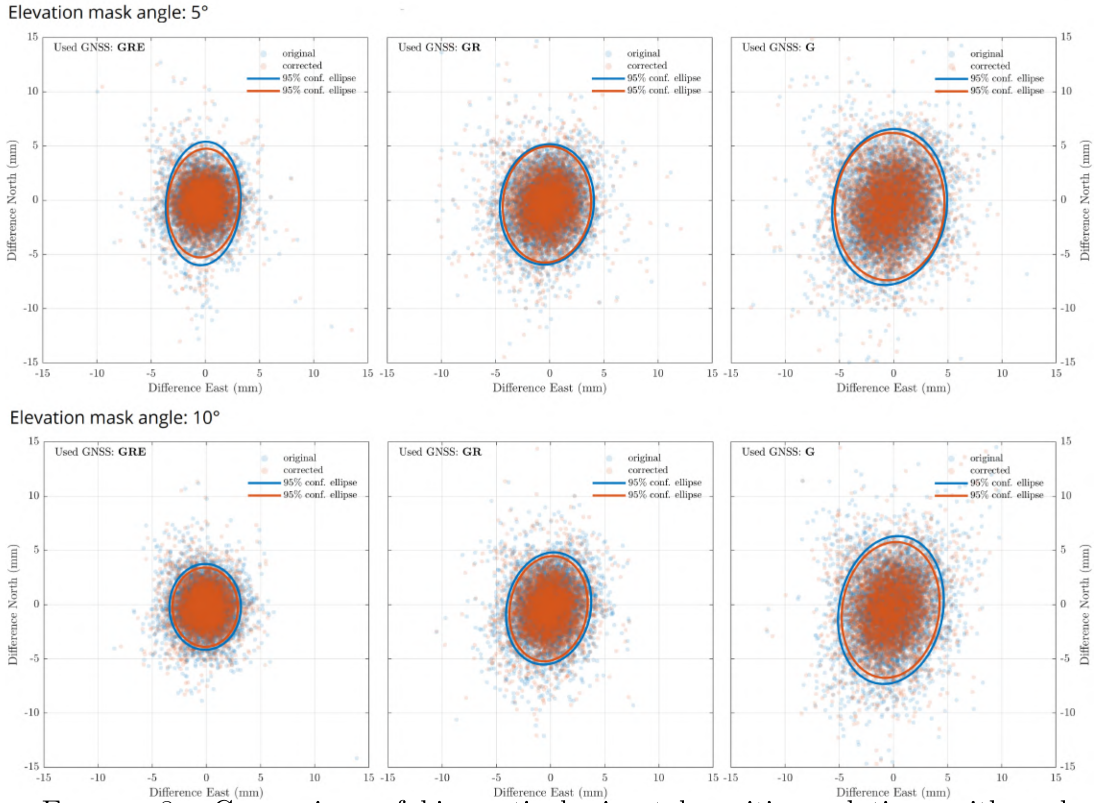

FIGURE 8: Comparison of kinematic horizontal position solutions with and without applied multipath correction for different GNSS and elevation mask angle.

4.2 Phase multipath detection using SNR combination

Phase multipath detection method using combination of SNR measurements, which will be discussed in this chapter, has been for the first time proposed in a paper (Strode and Groves, 2016). Idea behind this multipath detection method is relatively simple. It exploits relative phase of reflected signal $\Delta\Phi_{d,r}$, which plays important role in description of phase multipath as shown in section 3.2. Relative phase is defined by equation (2), so it depends on path delay Δd and carrier wavelength λ. For different carriers (e.g. L1, L2, L5 for GPS) we will obtain different relative phases $\Delta\Phi_{d,r}$, because of different wavelengths of the carriers. Because of different relative phases there will be subsequently also different effect on multipath error and also SNR values at each carrier frequency as it is shown in section 3.4.

Finding that the presence of phase multipath at site has different impact on SNR measurements at each of tracked carriers, exploded Strode and Groves into phase multipath detection method. Their method uses a test statistic S_a^s computed from current SNR measurements on different carriers. Computed test statistic is compared with threshold function which represents the limit of the system's performance under normal conditions (without multipath). If the test statistic exceed defined threshold, method marks the measurement as multipath-affected. SNR measurements at three different carrier frequencies are used to compute test statistic S_a^s. For GPS signals the test statistic S_a^s has the following form:

$$S_a^s = \sqrt{\left(\mathrm{SNR}_a^{s,L1} - \mathrm{SNR}_a^{s,L2} - \Delta\hat{C}_{12}(\varepsilon_a^s)\right)^2 + \left(\mathrm{SNR}_a^{s,L1} - \mathrm{SNR}_a^{s,L5} - \Delta\hat{C}_{15}(\varepsilon_a^s)\right)^2} \quad (16)$$

where $\mathrm{SNR}_a^{s,L1}$ denotes SNR measurement on GPS L1 carrier frequency for antenna a and satellite s. Terms $\Delta\hat{C}_{12}(\varepsilon_a^s)$, $\Delta\hat{C}_{15}(\varepsilon_a^s)$ represent reference functions which needs to be determined in advance during calibration measurement. Purpose of these reference functions is to model $\mathrm{SNR}_a^{s,L1} - \mathrm{SNR}_a^{s,L2}$, respectively $\mathrm{SNR}_a^{s,L1} - \mathrm{SNR}_a^{s,L5}$ differences under conditions where no multipath is present. Reference functions are modeled as a function of satellite elevation ε_a^s. Equation of test statistic (16) can be simplified to use only two frequencies as (17). We can expect that the detector in this form will be more susceptible to incorrect multipath identification because of less robustness. On the other hand this simplified formula will allow usage of the method on two-frequency receivers and open possibility to use GLONASS system as well as older GPS satellites.

$$S_a^s = \left| \mathrm{SNR}_a^{s,L1} - \mathrm{SNR}_a^{s,L2} - \Delta\hat{C}_{12}(\varepsilon_a^s) \right| \tag{17}$$

4.2.1 SNR calibration measurement

System (receiver and antenna) „normal“ performance need to be determined in low-multipath environment, in different words in environment where no objects are in close vicinity of antenna and no other than ground reflections are expected. Such measurement we can consider to be a calibration measurement and it will serve as reference for further multipath detection. Inevitable presence of ground reflections means that we are calibrating the system in a way it will expect only ground reflections and other reflections will be considered as multipath anomalies. The selection of calibration environment should be made with respect to the supposed usage of the system. It means that the calibration environment should be as close as possible to the environment where we will use GNSS system. For example if we intend to perform GNSS survey in urban area it is recommended to use calibration in environment with similar materials, e.g. open space bitumen parking lot. On the other hand if we want to perform the topographical survey in open country it is recommended to use flat grass-covered field.
The goal of calibration measurement is to determine reference functions for SNR values differences $\Delta\hat{C}_{12}(\varepsilon_a^s)$ and $\Delta\hat{C}_{15}(\varepsilon_a^s)$ in (16). Differences in SNR values at different carriers are caused by different: receiver antenna gain pattern, atmospheric attenuation, free-space loss and satellite antenna transmission pattern. All of these influences can be summed up and modelled together using low-order polynomials (up to order $n = 3$ are usually sufficient) to model SNR differences, since these are reasonable smooth functions.

In original method authors use all measured satellites to estimate reference functions $\Delta\hat{C}_{12}(\varepsilon_a^s)$ and $\Delta\hat{C}_{15}(\varepsilon_a^s)$. However we know that not all satellites in orbit are the same. They are grouped into satellites blocks and these can slightly differ between each other in term of signal strength or transmission antenna gain pattern. Good summary provides paper (Steigenberger et al., 2017). For this reason we may want to estimate reference functions separately for each satellite block, or even for each satellite. In later text we refer to these different SNR calibration modes as following:

- *all* – all satellites measured during calibration are used to estimate reference functions and S-statistic fit function.
- *block* – reference functions and S-statistic fit function are computed separately for each satellite block.
- *individual* – for each satellite we estimate its own reference functions and S-statistic fit function.

4.2.2 Finding threshold for detection S-statistic

Detection statistic S_a^s computed from calibration measurements by relations (16) or (17) is used to setup threshold T for later multipath detection. Similar to $\Delta\hat{C}$ function, also S_a^s is elevation dependent and is modeled as polynomial function of elevation. In (Strode and Groves, 2016) threshold T is computed as a function by fitting elevation dependent 3^{rd} order polynomial to S_a^s values and then added $t = 1, 2$ and 3-fold multiplication of fit RMS $\hat{\sigma}_S$. These three levels of threshold serve as multipath severity assessment. After application of this approach to calibration data from our calibration measurement, more than 3% of detection statistic S_a^s values were out of the most strict three-fold threshold function. For this reason we decided to edit threshold function by adding multiplicative elevation weighting function $\omega(\varepsilon)$ according to (18). Scaled exponential function has been chosen as weighing function. Argument in exponential function was further modified to contain also elevation mask angle ε_{cut} (in our calibration campaign $\varepsilon_{\text{cut}} = 10°$).

$$T_{tw\sigma}(\varepsilon) = \hat{S}_a^s(\varepsilon) + \underbrace{\beta \cdot \exp\left(\frac{90° - \varepsilon}{90° - \varepsilon_{\text{cut}}}\right)}_{\omega(\varepsilon)} \cdot t \cdot \hat{\sigma}_S \tag{18}$$

Proposed weighting function $\omega(\varepsilon)$ is scaled by β factor, which was computed according procedure described in Fig. 9 by iterative process with increment $\Delta\beta = 0.001$. Final estimated $\hat{\beta}$ factor is used in (18) and for $t = 3$ we got 99.9% below threshold line. Such threshold function was later used for multipath detection.

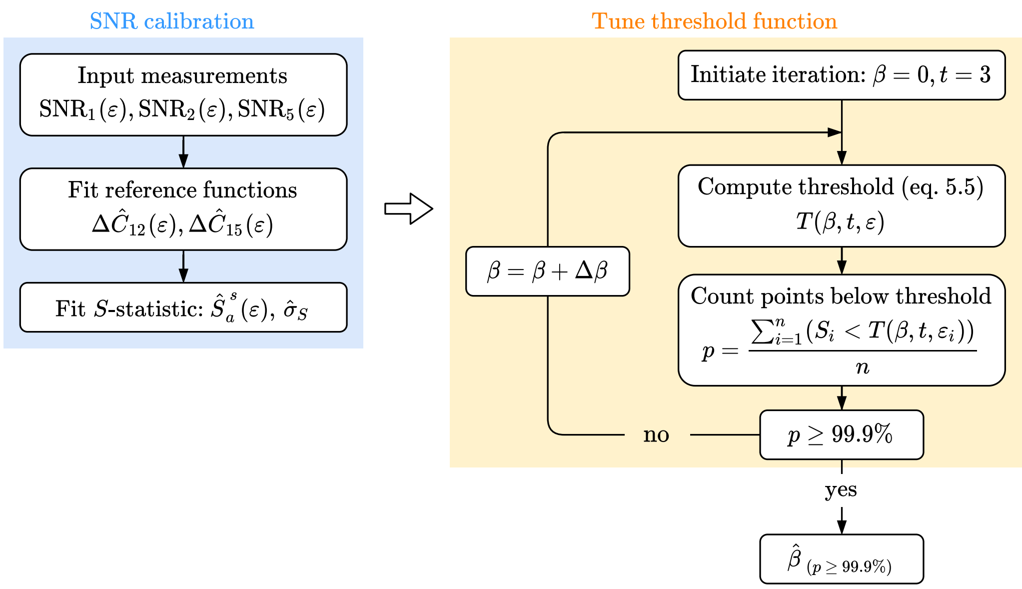

FIGURE 9: Procedure for SNR calibration and estimation of β factor.

4.2.3 Calibration measurement campaign

For calibration purpose observations from open field environment with low vegetation grow has been taken. Observation took place near Vajnory, Slovakia on October 7, 2016. Combined geodetic GNSS receiver Trimble R8 Model 3 was used with tracking capability of GPS, Galileo and GLONASS systems at 1s sampling. Totally 15 GPS satellites and 9

GLONASS satellites were used to estimate polynomial coefficients of $\Delta\hat{C}_{12}$, $\Delta\hat{C}_{15}$ functions as a function of satellite elevation. Only data with elevation above 10 degrees were used. Linear and parabolic trend functions $\Delta\hat{C}$ has been found as sufficient to appropriate fit measured data. Calibration reference functions were estimated for GPS 3-frequency as well as for GPS 2-frequency measurements and for GLONASS 2-frequency. For each system and frequency combination there were estimated three different sets of reference functions for: all satellites together, grouped according satellite blocks and individually for each satellite.

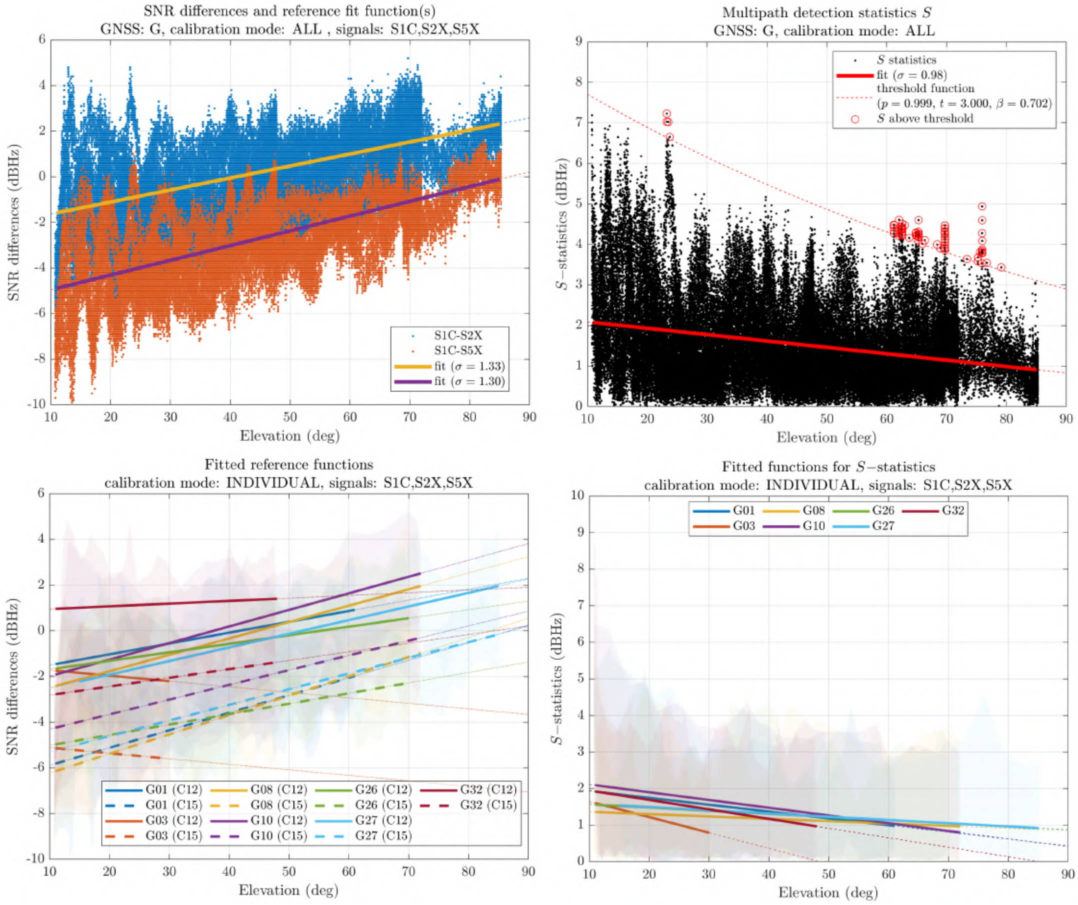

FIGURE 10: Estimated reference functions $\Delta\hat{C}_{12}$, $\Delta\hat{C}_{15}$ and fit of S-statistic for GPS 3-frequencies (all/individual satellite strategy)

4.2.4 Multipath detection in urban environment

To test introduced method of multipath detection we made an experimental GNSS static measurement in urban environment. As a test site we chose Slovak University of Technology principal residence. There is the open courtyard inside building block as it is shown on Fig. 11. Big walls of surrounding, up to 25 m high buildings, should introduce many reflections. We used the same equipment as during calibration measurement. Data were logging at 1s sampling rate for 16 hours on 26 April, 2017.

For measured data detection statistics S_a^s for each epoch and each tracked satellite were computed according to equation (16) or (17). To find out multipath infected signals we have compared detection S-statistic values to the threshold function (18). If the S-statistic is greater than threshold function value then we consider tested signal in given epoch as multipath and is excluded from further processing. To better visually asses possible reflections we used zenith-pointing image panorama taken at site. Panorama was

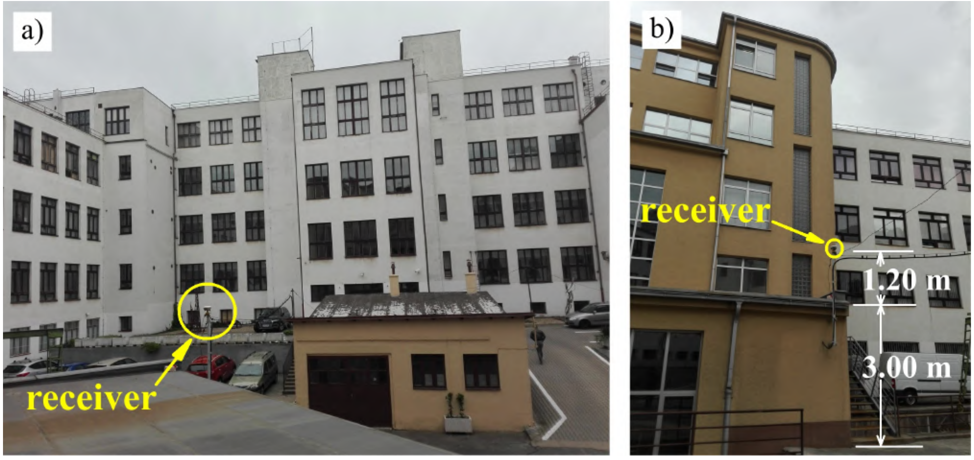

FIGURE 11: Experimental site at SUT principal residence. Antenna was placed on the steel rod approximately 4.20 m above ground (1.20 m above reduced roof) and 5 meters off the nearest wall. The South (a) and North-East view (b).

created from the series of images with given orientation in open-source photo stitching software Hugin. Proper level and orientation to geographic north was ensured during photographing using the survey tribrach. It is obvious that if there is tracked signal of satellite which is located „inside" building on the panorama then this signal has to pass by one or more reflection from building walls. In case that the satellite signal is tracked close to building roof edge, it is possible that the signal was diffracted. In both cases, this signal would be corrupted and should be identified by detection. Test results for all three approaches: a) all satellites calibration, b) satellite block calibration, c) individual satellite calibration, can be seen on skyplot graphic on Fig. 12. Each dot in this plot represent measured satellite with all available measurements at given epoch and yellow dots represent detected multipath. Satellite positions with incomplete measurement epochs (e.g. only C1 measurement for GPS) are not shown on the figure. From available panorama photo, building mask was created and used as reference for different calibration modes. For all observation data handling we use MATLAB functions from developed GNSS-toolbox. These functions enable to load RINEX files and compute satellite positions. Toolbox functions can also perform detection of multipath based on S-statistic and removal of such measurement from RINEX file. Modified RINEX files for all SNR calibration modes were exported for further processing. Test site position was estimated with RTKLIB software in kinematic mode. As reference site we use SUT1 permanent station located at Slovak University of Technology, which is around 400 metres away from our test site.

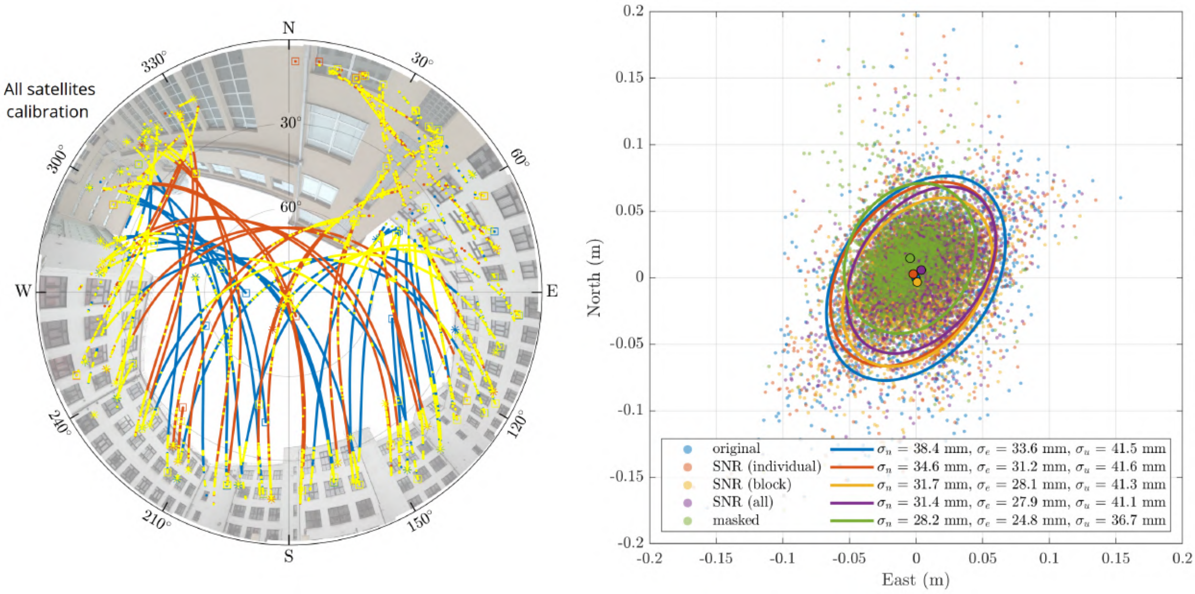

FIGURE 12: Skyplot graphics of test measurement multipath detection results. Blue color represent GPS satellites, red color are GLONASS. Yellow dots represents measurements marked as multipath which were excluded from further processing.

Estimated positions differences are shown on Fig. **??**. Position computed from original/not modified data were taken as reference. Biggest improvement in term of standard deviation against original measurements we can see for scenario where we excluded measurements based on building mask (improvement about 26% for horizontal position and about 11% for height). From different SNR calibration modes, best performance is achieved with SNR calibration mode where we use all satellites to get reference functions and S-statistic values fit (improvement about 18% for position and minor improvement of 1% for height). From skyplot views on Fig. 12 we can see that some satellites for block/individual satellite SNR calibration mode in the open sky were almost fully removed. Also exclusion of measurements from north-east part, where it seems most of the reflection comes, is best for all satellite calibration mode. This can partially explain almost no improvement in height estimates and lower improvement in position estimates for block/individual calibration modes.

Contributions of the thesis

We recognized following outputs as scientific contributions of the thesis:

1. We have proposed procedure to estimate multipath correction map at given site using double-differenced phase residuals with auxiliary site setup.
2. We have proposed simplified version of SNR detector which can be used for different GNSS systems. New approach with estimation of reference functions separately for block/individual satellites was explored.
3. We have developed and made publicly available MATLAB based GNSS-toolbox, which contains set of classes, functions and example scripts used for reading and processing of GNSS related data. Toolbox contains procedures to read standard files used in GNSS processing chain such as RINEX, SP3, ANTEX and ANUBIS XTR files. It implements SNR phase multipath detection method described in chapter 5.2. Advantage of the toolbox is object-oriented code style, which is suitable for further enhancements.

Practical contributions of the thesis can be summarized as following:

1. We have computed and applied multipath correction map for JABO GNSS permanent site which shows improvements in positioning precision and and ambiguity fixes.
2. We have proposed and construct portable shield from radio-frequency absorbing foam to reduce multipath on site.
3. We have estimated SNR calibration reference functions for different calibration modes (all/block/individual).
4. We have performed measurement and multipath detection in urban environment with SNR multipath detector. Discarding measurements marked as multipath shows improvements in positioning precision.

Concluding remarks

In the thesis we have shown two separate methods to identify phase multipath errors which rely purely on GNSS observables. Method based on double-differenced residuals rely on setup of auxiliary temporal site close to objective site and requires assumption of no multipath at this temporal site. For that reason portable shield from radio-frequency absorption foam was necessary to reduce effect of ground reflections. Verification measurement with and without absorption foam shield shows reduction of SNR values variability by about 30% for a case when shield was deployed. Based on the datasheet information there was expected higher attenuation, but we think that bigger structure or more layers of absorption foam may improve this. Anyway our test verification prove utility of such setup for observations where acquisition of multipath-free measurement is required, such the one used for computation of double difference phase residuals.

Experiment at JABO site show that even with absence of dominant reflector multipath effect can become non-negligible. We can see that several close-by service installations at JABO site, such as railings, steel masts or antennas can introduce significant multipath footprint. Method of multipath correction map may bring benefits for continuously operating permanent stations where additional infrastructure is already installed and cannot be removed. Any user using this station as reference then could benefit from such improvement. Some correction grids (e.g. GPS L5 or Beidou) would require more days of observation to be improved. Encouraged by results from testing of SNR detection in urban experiment where we noticed significant improvement after applying mask of surrounding buildings, we would suggest to apply such visibility mask also on permanent sites, even when we do not expect such big improvement like in our test site in urban environment.

Multipath detector based on SNR measurements shows promising results in our experiment in urban environment. Results for block and individual satellite SNR calibration are to our surprising bit worse than results obtained for all satellites SNR calibration. We think that it can be improved with longer calibration session. Performance of the SNR multipath detector is good even when we use calibration from different environment (open field during calibration vs. urban environment in test). For that reason we are positive about further improvement in robustness of this method. Also modelling of reference functions with other than polynomial functions, e.g. splines or non-parametric moving averages may be objective for further studies.

Bibliography

Bilich, A. and Larson, K. M. (2008). Mapping the GPS multipath environment using the signal-to-noise ratio (SNR). *Radio Science*, 42.

Bilich, A., Larson, K. M., and Axelrad, P. (2008). Modeling GPS phase multipath with SNR: Case study from the Salar de Uyuni, Boliva. *Journal of Geophysical Research*, 113:12.

Bishop, G. J., Klobuchar, J. A., and Doherty, P. H. (1985). Multipath effects on the determination of absolute ionospheric time delay from GPS signals. *Radio Science*, 20(3):388–396.

Comp, C. and Axelrad, P. (Jan./1998). Adaptive SNR-based carrier phase multipath mitigation technique. *IEEE Transactions on Aerospace and Electronic Systems*, 34(1):264–276.

Dach, R., Lutz, S., Walser, P., and Fridez, P. (2015). Bernese GNSS Software Version 5.2. Astronomical Institute, University of Bern.

Dilssner, F., Seeber, G., Wübbena, G., and Schmitz, M. (2008). Impact of Near-Field Effects on the GNSS Position Solution. In *Proceedings of the 21st International Technical Meeting of the Satellite Division of The Institute of Navigation*, pages 612–624, Savannah, GA, USA.

Elósegui, P., Davis, J. L., Jaldehag, R. T. K., Johansson, J. M., Niell, A. E., and Shapiro, I. I. (1995). Geodesy using the Global Positioning System: The effects of signal scattering on estimates of site position. *Journal of Geophysical Research*, 100(B7):9921–9934.

Estey, L. H. and Meertens, C. M. (1999). TEQC: The Multi-Purpose Toolkit for GPS/GLONASS Data. *GPS Solutions*, 3(1):42–49.

Evans, A., Herman, B., Coco, D., and Clynch, J. (1986). Comparsion of GPS pseudo range and biased Doppler range measurements to demonstrate signal multipath effects. In *Proceedings of 4th International Symposium on Satellite Positioning*, Austin, Texas.

Fan, K. and Ding, X. (2006). Estimation of GPS Carrier Phase Multipath Signals Based on Site Environment. *Journal of Global Positioning Systems*, 5(1&2):22–28.

Fenton, P. C. and Townsend, B. R. (1994). The Multipath Estimating Delay Lock Loop: Approaching Theoretical Accuracy Limits. In *Proceedings of 1994 IEEE Position*, pages 246–251.

Georgiadou, P. and Kleusberg, A. (1988). On carrier signal multipath effects in relative GPS positioning. *Manuscripta geodaetica*, 13(3):172–179.

Gerhatova, L., Hefty, J., and Spanik, P. (2016). Short-Term and Long-Term Variability of Antenna Position Due to Thermal Bending of Pillar Monument at Permanent GNSS Station. *Reports on Geodesy and Geoinformatics*, 100(1):67–77.

Hofmann-Wellenhof, B., Lichtenegger, H., and Wasle, E. (2008). *GNSS - Global Navigation Satellite Systems: GPS, GLONASS, Galileo, and More*. Springer, Wien ; New York.

Kaplan, E. D. and Hegarty, C. J. (2006). *Understanding GPS: Principles and Applications*. Artech House, second edition.

Kerkhoff, A., Harris, R. B., Petersen, C. P., and Pickard, A. (2010). Modifications to GPS Reference Station Antennas to Reduce Multipath. In *23rd International Technical Meeting of the Satellite Division of The Institute of Navigation*, pages 866–878, Portland, OR, USA.

Kouba, J. (2009). A guide to using international GNSS service (IGS) products. Technical report, Natural Resources Canada, Geodetic Survey Division, 615 Booth Street, Ottawa, Ontario.

Langley, R. B. (1997). GPS Receiver System Noise. *GPS World*, pages 40–45.

Lau, L. and Cross, P. (2006). A New Signal-to-Noise-Ratio Based Stochastic Model for GNSS High-Precision Carrier Phase Data Processing Algorithms in the resence of Multipath Errors. In *ION GNSS*, pages 276–285, Fort Worth, Texas, USA.

Lau, L. and Cross, P. (2007). Development and testing of a new ray-tracing approach to GNSS carrier-phase multipath modelling. *Journal of Geodesy*, 81(11):713–732.

Leick, A. (2004). *GPS Satellite Surveying - Third Edition*. John Wiley & Sons, Inc., third edition.

Misra, P. and Enge, P. (2011). *Global Positioning System: Signals, Measurements, and Performance*. Ganga-Jamuna Press.

Moreau, J., Ambellouis, S., and Ruichek, Y. (2017). Fisheye-Based Method for GPS Localization Improvement in Unknown Semi-Obstructed Areas. *Sensors*, 17(12):119.

Nicolas, M. L., Jacob, M., Smyrnaios, M., Schon, S., and Kurner, T. (2011). Basic concepts for the modeling and correction of GNSS multipath effects using ray tracing and software receivers. In *2011 IEEE-APS Topical Conference on Antennas and Propagation in Wireless Communications*, pages 890–893, Torino. IEEE.

Rost, C. and Wanninger, L. (2009). Carrier phase multipath mitigation based on GNSS signal quality measurements. *Journal of Applied Geodesy*, 3(2).

Špánik, P. (2015). *Analýza meraní družíc GPS a Galileo z hľadiska detekcie, modelovania a vizualizácie efektu viacsmerného šírenia signálov*. Master thesis, Slovenská Technická Univerzita v Bratislave, Bratislava.

Špánik, P. (2016). Efekt fázového multipathu v meraniach GNSS. In *Advances in Architectural, Civil and Environmental Engineering*, Bratislava, Slovakia.

Špánik, P. (2017). GNSS Phase Multipath Effect In Single Reflector Environment. In *Juniorstav 2017*, page 10, Brno, Česká republika. ECON publishing, s.r.o.

Špánik, P. (2018). Analýza efektu viaccestného Šírenia sa signálu na permanentných staniciach SKPOS. In *Advances in Architectural, Civil and Environmental Engineering*, Bratislava, Slovakia.

Špánik, P., García-Asenjo, L., and Baselga, S. (2019a). Optimal combination and reference functions of signal-to-noise measurements for GNSS multipath detection. *Measurement Science and Technology*, 30(4):044001.

Špánik, P. and Gerhátová, Ľ. (2016). Detekcia efektu multipath v meraniach GNSS. In *Družicové Metody v Geodézii a Katastru*, Brno, Česká republika. ECON publishing, s.r.o.

Špánik, P., Gerhátová, Ľ., and Janák, J. (2016). Vizualizácia výsledkov geodetických meraní s použitím programového balíka Generic Mapping Tools. *Cartographic letters*, 24(1):23–34.

Špánik, P. and Hefty, J. (2017). Multipath detection with the combination of SNR measurements – Example from urban environment. *Geodesy and Cartography*, 66(2).

Špánik, P., Hefty, J., Gerhátová, Ľ., and Papčo (2018). Prvé skúsenosti so spracovaním raw GNSS dát zo zariadení so systémom Android. In *Družicové Metody v Geodézii a Katastru*, page 8, Brno, Česká republika. ECON publishing, s.r.o.

Špánik, P., Papčo, J., Gerhátová, Ľ., and Hefty, J. (2019b). Analýza efektu multipath z permanentných meraní s využitím rôznych GNSS. In *Družicové Metody v Geodézii a Katastru*, page 5, Brno, Česká republika. ECON publishing, s.r.o.

Steigenberger, P., Thoelert, S., and Montenbruck, O. (2017). GNSS satellite transmit power and its impact on orbit determination. *Journal of Geodesy*.

Strode, P. R. R. and Groves, P. D. (2016). GNSS multipath detection using three-frequency signal-to-noise measurements. *GPS Solutions*, 20(3):399–412.

Suzuki, T. and Kubo, N. (2015). Simulation of GNSS Satellite Availability in Urban Environments Using Google Earth. In *Proceedings of the ION 2015 Pacific PNT Meeting*, pages 1069–1079, Honolulu, Hawaii, USA.

Takasu, T. (2013). RTKLIB: An open source program package for GNSS positioning.

Teunissen, P. J. and Montenbruck, O., editors (2017). *Springer Handbook of Global Navigation Satellite Systems*. Springer International Publishing, Cham.

Tongleamnak, S. and Nagai, M. (2017). Simulation of GNSS Availability in Urban Environments Using a Panoramic Image Dataset. *International Journal of Navigation and Observation*, 2017:1–12.

Townsend, B. R., Fenton, P. C., Van Dierendonck, K. J., and Van Nee, R. D. J. (1995). L1 carrier phase multipath error reduction using MEDLL technology. In *Proceedings of ION*, Palm Springs, California.

US Department of Defence (2013). *GPS Interface Specification IS-GPS-200H.* Global Positioning Systems Directorate Systems Engineering & Integration.

Vaclavovic, P. and Douša, J. (2013). ANUBIS – a tool for quality check of multi-GNSS observation and navigation data. In *4th International Colloquium Scientific and Fundamental Aspects of the Galileo Programme*, page 6, Prague, Czech Republic.

Wanninger, L. and May, M. (2001). Carrier-Phase Multipath Calibration of GPS Reference Stations. *Journal of The Institute of Navigation*, 48(2):113–124.

Wübbena, G., Schmitz, M., and Prüllage, A. (October 10 - 11, 2011). On GNSS station calibration of near-field multipat in RTK networks. In *International Symposium on GNSS, Space-Based and Ground-Based Augmentation Systems and Applications*, page 6, Berlin, Germany.

Yang, H., Yang, X., Sun, B., and Su, H. (2016). Global Navigation Satellite System Multipath Mitigation Using a Wave-Absorbing Shield. *Sensors*, 16(12):1332.

Publications of the author

Journal articles (refereed)

Špánik, P., García-Asenjo, L., and Baselga, S. (2019a). Optimal combination and reference functions of signal-to-noise measurements for GNSS multipath detection. *Measurement Science and Technology*, 30(4):044001

Špánik, P., Gerhátová, Ľ., and Janák, J. (2016). Vizualizácia výsledkov geodetických meraní s použitím programového balíka Generic Mapping Tools. *Cartographic letters*, 24(1):23–34

Gerhatova, L., Hefty, J., and Spanik, P. (2016). Short-Term and Long-Term Variability of Antenna Position Due to Thermal Bending of Pillar Monument at Permanent GNSS Station. *Reports on Geodesy and Geoinformatics*, 100(1):67–77

Špánik, P. and Hefty, J. (2017). Multipath detection with the combination of SNR measurements – Example from urban environment. *Geodesy and Cartography*, 66(2)

Conference articles (refereed)

Špánik, P., Papčo, J., Gerhátová, Ľ., and Hefty, J. (2019b). Analýza efektu multipath z permanentných meraní s využitím rôznych GNSS. In *Družicové Metody v Geodézii a Katastru*, page 5, Brno, Česká republika. ECON publishing, s.r.o.

Špánik, P., Hefty, J., Gerhátová, Ľ., and Papčo (2018). Prvé skúsenosti so spracovaním raw GNSS dát zo zariadení so systémom Android. In *Družicové Metody v Geodézii a Katastru*, page 8, Brno, Česká republika. ECON publishing, s.r.o.

Špánik, P. (2018). Analýza efektu viaccestného Šírenia sa signálu na permanentných staniciach SKPOS. In *Advances in Architectural, Civil and Environmental Engineering*, Bratislava, Slovakia

Špánik, P. (2017). GNSS Phase Multipath Effect In Single Reflector Environment. In *Juniorstav 2017*, page 10, Brno, Česká republika. ECON publishing, s.r.o.

Špánik, P. and Gerhátová, Ľ. (2016). Detekcia efektu multipath v meraniach GNSS. In *Družicové Metody v Geodézii a Katastru*, Brno, Česká republika. ECON publishing, s.r.o.

Špánik, P. (2016). Efekt fázového multipathu v meraniach GNSS. In *Advances in Architectural, Civil and Environmental Engineering*, Bratislava, Slovakia

Špánik, P. and Hefty, J. (2015). Tvorba aplikácie na modelovanie a vizualizáciu efektu viacsmerného šírenia družicových signálov. In *Geodetické základy a geodynamika 2015*, Kočovce, Slovakia. pages 10-18. ISBN 978-80-227-4466-9.

Abstracts and posters

Špánik, P. and Hefty, J. (2017). Multipath detection using SNR values for Galileo satellites. In *6th International Colloqium on Scientific and Fundamental Aspects of GNSS/Galileo*. Valencia, Spain, October 25-27.

Špánik, P., Hefty, J., Gerhátová, Ľ. and Papčo, J. (2017). Multipath Detection with Three-frequency SNR Combination – Example from Urban Environment. In *EUREF Symposium 2017*, Wroclaw, Poland, May 17-19

Gerhátová, Ľ., Špánik, P. and Hefty, J. (2016). Možnosti vizualizácie prejavov zemetrasení na mape. In *Kartografická konferencia 2016*. Bratislava, Slovakia, October 20-21

Citations

Špánik, P., García-Asenjo, L., and Baselga, S. (2019a). Optimal combination and reference functions of signal-to-noise measurements for GNSS multipath detection. *Measurement Science and Technology*, 30(4):044001

1. Yiran, L., Li, J. Chunyang, Y., Bing, X., You, L., Li-Ta, H. and El-Sheimy, N. (2019). Research on Time-Correlated Errors Using Allan Variance in a Kalman Filter Applicable to Vector-Tracking-Based GNSS Software-Defined Receiver for Autonomous Ground Vehicle Navigation. In *Remote Sensing*, vol. 11, no. 9, ISSN 2072-4292.
2. Mingkun S., Yanxi Y., Lei Q., Xuyang T. and Huina S. (2020). Enhanced multipath mitigation method based on multi-resolution CNR model and adaptive statistical test strategy for real-time kinematic PPP. In *Advances in Space Research*, Volume 67, Issue 2, 2021, Pages 868-882, ISSN 0273-1177, https://doi.org/10.1016/j.asr.2020.10.035.
3. Xia Y., Pan S., Meng X., Gao W. and Wen H. (2020). Robust Statistical Detection of GNSS Multipath Using Inter-Frequency C/N_0 Differences. In *Remote Sensing*. 2020; 12(20):3388. https://doi.org/10.3390/rs12203388.
4. Ren Z., Kuang C. and Zhang Z. (2020). Phase Multipath Detection and Its Effect on Positioning Based on Multi-GNSS. In: *China Satellite Navigation Conference Proceedings: Volume II*. CSNC 2020. Lecture Notes in Electrical Engineering, vol 651. Springer, Singapore. https://doi.org/10.1007/978-981-15-3711-0_27.
5. Paziewski, J. and Crespi, M. (2020). High-precision multi-constellation GNSS: methods, selected applications and challenges. In Measurement Science and Technology, Volume 31, Issue 1. https://doi.org/10.1088/1361-6501/ab20a6.

Gerhatova, L., Hefty, J., and Spanik, P. (2016). Short-Term and Long-Term Variability of Antenna Position Due to Thermal Bending of Pillar Monument at Permanent GNSS Station. *Reports on Geodesy and Geoinformatics*, 100(1):67–77

1. Mocnik, R., Koler, B., Zupan, D. and Ambrozic, T. (2019). Investigation of the Precision in Geodetic Reference-Point Positioning Because of Temperature-Induced Pillar Deflections. In *Sensors*, vol. 19, no. 16.

Špánik, P. and Hefty, J. (2017). Multipath detection with the combination of SNR measurements – Example from urban environment. *Geodesy and Cartography*, 66(2)

1. Zhan, Y., Zeng, G. and Duan C. (2021). A High Order Statistics Based Multipath Interference Detection Method. in *IET Communications*, April 8, 2021, https://doi.org/10.1049/cmu2.12171.

2. Uaratanawong, V., Satirapod, Ch. and Tsujii, T. (2021). Evaluation of multipath mitigation performance using signal-to-noise ratio (SNR) based signal selection methods. In *Journal of Applied Geodesy*, vol. 15, no. 1, 2021, pp. 75-85. https://doi.org/10.1515/jag-2020-0045.

3. Ollander, S., Bode, F. and Baum, M. (2020). Multipath Delay Estimation Using Signal Power Measurements from Multiple Carrier Frequencies, In *2020 International Conference on Localization and GNSS (ICL-GNSS)*. pp. 1-5, doi: 10.1109/ICL-GNSS49876.2020.9115535.

4. Bažec, M., Dimc, F. and Pavlovčič-Prešeren, P. (2020). Evaluating the Vulnerability of Several Geodetic GNSS Receivers under Chirp Signal L1/E1 Jamming. In *Sensors* 2020; 20(3):814. https://doi.org/10.3390/s20030814.

5. Ollander, S., Bode, F. and Baum, M. (2019). The Dual-frequency Post-correlation Difference Feature for Detection of Multipath and non-Line-of-Sight Errors in Satellite Navigation. In *22th International Conference on Information Fusion (FUSION)*. pp. 1-8. https://ieeexplore.ieee.org/document/9011302

6. Ollander, S. Bode, F. and Baum, M. (2018). Multi-frequency GNSS signal fusion for minimization of multipath and non-line-of-sight errors: A survey. In *15th Workshop on Positioning, Navigation and Communications.*

7. Yajun, F., Wang, P., Yu, J., Wang, S., Yu, W., Li, J., Yan, N., He, D. and Chen, X. (2018). Accuracy Analysis on the Beidou/INS Integrated Navigation based on the Field Trial. In *IEEE 23rd International Conference on Digital Signal Processing (DSP)*, ISSN 1546-1874.